ADVANCED FUNCTIONAL MATERIALS
www.afm-journal.de

Tuning Electronic and Ionic Transport by Carbon-Based Additives in Polymer Electrolytes for Thermoelectric Applications

Maximilian Frank and Jens Pflaum**

Thermoelectric materials utilizing ionic transport open-up entirely new possibilities for the recuperation of waste heat. Remarkably, solid state electrolytes which have entered the focus of battery research in recent years turn-out to be promising candidates also for ionic thermoelectrics. Here, the dynamics of ionic transport and thermoelectric properties of a methacrylate based polymer blend in combination with a lithium salt is analyzed. Impedance spectroscopy data indicates the presence of just one transport mechanism irrespective of lithium salt concentration. In contrast, the temperature dependent ionic conductivity increases with salt concentration and can be ascribed to a Vogel–Fulcher–Tammann (VFT) behavior. The obtained Seebeck coefficients of 2 mV K^{-1} allow for high power outputs while the polymer matrix maintains the temperature gradient by its low thermal conductivity. Adding multi-walled carbon nanotubes to the polymer matrix allows for variation of the Seebeck coefficient as well as the ionic and electronic conductivities. As a result, a transition between a high temperature VFT regime and a low temperature Arrhenius regime appears at a critical temperature, T_c, shifting upon addition of salt. The observed polarity change in Seebeck voltage at T_c suggests a new mode of thermoelectric operation, which is demonstrated by a proof-of-concept mixed electronic-ionic-thermoelectric generator.

1. Introduction

Ionic transport constitutes a key process in organic-based electrochemical energy storage. As such, much work on the electrochemical device performance is devoted to cyclability, energy density, and conductivity. Vice versa, the ionic transport characteristics of these materials offer intriguing possibilities for their utilization in thermoelectrics (TE) to recuperate substantial amounts of waste heat into electrical power.[1] Efficient TE applications desire for materials with large Seebeck coefficient, S, high electrical conductivity, σ, and low thermal conductivity, κ. These parameters are commonly interrelated by the dimensionless figure-of-merit at given temperature $zT = S^2\sigma T\kappa^{-1}$. With regard to achieving high power factors, defined as $PF = S^2\sigma$,[2] in purely electronic systems, however, the two most impactful parameters of TE transport, S and σ, are quite often in conflict as they are anti-correlated. Hence, it is of great interest to optimize the TE parameters selectively and—if possible—decoupled from each other. Different approaches like doping,[3,4] incorporation of additives such as low-dimensional molecular metals,[5] organic charge transfer salts,[6] or carbon nanotubes[7] have been reported in literature.[8,9] But, despite tremendous efforts in recent years, the Seebeck coefficient in polymer materials with neat electronic conductivity remains quite low, only a few 10 μV K^{-1}.[10–12] The main reason for this limitation is given by the dependence of S on the charge carrier concentration. In materials with ionic transport, however, the lower charge carrier mobility causes lower conductivity and therefore enhanced Seebeck coefficients S. As such, solid polymer electrolytes (SPE) with thermovoltages in the mV range would offer an excellent alternative to materials showing only electronic transport.[13–15] Therefore, it is imperative that insights in the microscopic processes governing ion conduction and quantitative information on the related transport parameters are needed to further optimize the electrical behavior for example, by adjusting the energetics or structural properties of the host material. Lithium-based electrolytes in battery research are available in large quantities and are solution processable hence allowing for large scale implementation.[16,17] Both areas of scientific activity, battery research, and thermoelectric research, respectively, can mutually benefit from the results and the increasing knowledge of the investigated material systems. In this work, by using an electrolyte with a high room temperature ionic conductivity of about 10^{-3} S m^{-1} proposed for lithium battery application,[18] we demonstrate the

M. Frank, J. Pflaum
Experimental Physics VI
Julius-Maximilian University
D-97074 Würzburg, Germany
E-mail: maximilian.frank@physik.uni-wuerzburg.de;
jpflaum@physik.uni-wuerzburg.de
J. Pflaum
Bavarian Center for Applied Energy Research (ZAE Bayern)
D-97074 Würzburg, Germany

The ORCID identification number(s) for the author(s) of this article can be found under https://doi.org/10.1002/adfm.202203277.

DOI: 10.1002/adfm.202203277

tuning of electrical and ionic transport properties by varying the contents of lithium salt and carbon-nanotube additive, respectively. This approach leads to high Seebeck coefficient of about $2\,mV\,K^{-1}$ on macroscopic scales of several millimeters, which refer to realistic dimensions of thermoelectric generators (TEG) and are necessary to maintain a decent temperature gradient.[19] By means of a prototypical TEG, we illustrate new functionalities offered by such an electronic-ionic-transport based device.

2. Results and Discussion

We chose the solid state polymer matrix poly(ethylene glycol)-methacrylate (PEGMA) : bisphenol-A-ethoxylate-dimethacrylate (BEMA) w/w 3:7 with variable concentrations of lithium bis(trifluoromethane)-sulfonimide (LiTFSI) as starting point for our thermoelectric characterization. This solid polymer electrolyte shows a very high thermal stability up to 300 °C[18] which enables thermoelectric generators recovering waste heat in the technologically relevant mid-temperature regime. Moreover, from a preparational point of view, the viscosity of the unhardened electrolyte offers printing-based fabrication and, in combination with the rapid UV-curing of the polymer, an easy up-scaling.

2.1. Thermoelectric Characterization

In a first set of studies, the thermovoltage U_{th} has been measured as function of LiTFSI salt concentration. Three samples have been prepared with concentrations $c_{LiTFSI} = 0.0\,mol\,kg^{-1}$ (SPE0), $0.2\,mol\,kg^{-1}$ (SPE2), and $0.5\,mol\,kg^{-1}$ (SPE5), respectively. A representative curve of U_{th} versus applied temperature gradient ΔT at room temperature is shown for sample SPE2 in **Figure 1**a. From the slope of the linear fit to the data a Seebeck coefficient of $S = (-0.96 \pm 0.01)\,mV\,K^{-1}$ can be deduced. The driving force of this ion-related thermoelectric effect is provided by the applied temperature gradient across the electrolyte which leads to ion movement toward the cold side, hence, building up a charge concentration gradient, a phenomenon termed Soret-effect. In an electrolyte where cations and anions can thermodiffuse similarly, that is, where ions of opposite sign neutralize each other, no effective thermovoltage will arise. Thus, in the material combinations investigated here, Li^+ cations cannot move as easily as the much bigger $TFSI^-$ anions. Though counterintuitively at first sight, this can be explained by the cations' propensity to bind to the electronegative polymer backbone. This process is corroborated by a transport number of $t_+ = 0.4$ reported in literature[20] which is effectively the ratio of the mobilities of the ions ($t_+ = \mu_+/(\mu_+ + \mu_-)$) indicating that the current through the polymer electrolyte is preferentially carried by anions. Hence, the excess of anions that is piled up at the cold side generates a thermovoltage U_{th} of negative polarity. As the Soret effect is the primary mechanism, we anticipate a large gradient in unbalanced ion concentration to be benefical for a maximum thermovoltage build-up, that is, high Seebeck coefficient. Hence, an electrolyte offering either a transport number of $t_- = 1$ or $t_+ = 1$, that is, a maximum unbalanced contribution of anions and cations to conductivity across the electrolyte, is expected best for thermoelectric applications. This, however is in contrast to battery applications where only the highest possible lithium transport number of $t_+ = 1$ is demanded.[21] Seebeck coefficients as function of device temperature are plotted in Figure 1b for the three samples SPE0 (teal pentagons), SPE2 (blue diamonds), and SPE5 (green dots). Sample SPE0 without any additives in the polymer, exhibits a room temperature Seebeck coefficient of $S = (-0.14 \pm 0.12)\,mV\,K^{-1}$, which agrees well with the expected range for untreated conducting polymers.[10,22] Adding LiTFSI salt at a concentration of $c_{LiTFSI} = 0.2\,mol\,kg^{-1}$ to the matrix (sample SPE2) increases the Seebeck coefficient to $S = (-0.96 \pm 0.01)\,mV\,K^{-1}$. Higher LiTFSI concentrations, for example, $c_{LiTFSI} = 0.5\,mol\,kg^{-1}$ (sample

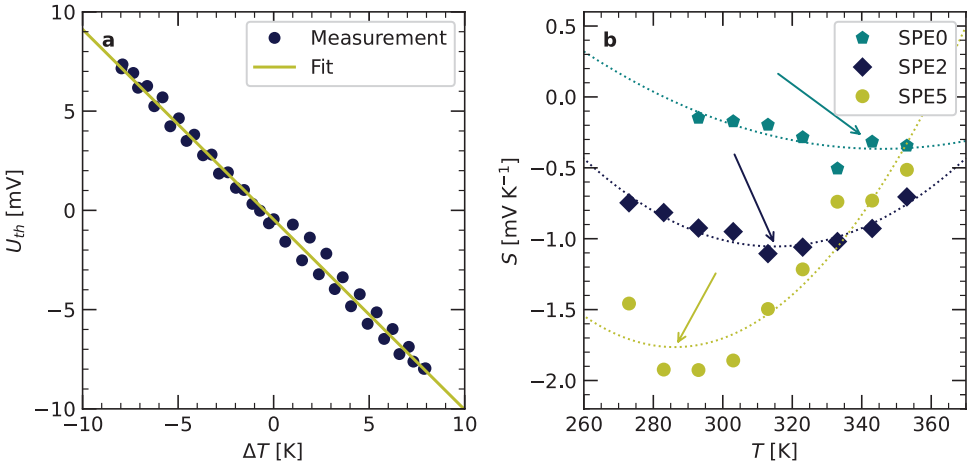

Figure 1. a) Thermovoltage U_{th} versus temperature difference ΔT across the solid polymer electrolyte measured for a LiTFSI salt concentration of $c_{LiTFSI} = 0.2\,mol\,kg^{-1}$ (sample SPE2) at room temperature. The slope of the linear fit to the data yields a Seebeck coefficient of $S = (-0.96 \pm 0.01)\,mV\,K^{-1}$. The data has been corrected for parasitic offset voltages. b) Seebeck coefficient S as a function of device temperature for different concentrations $c_{LiTFSI} = 0.0\,mol\,kg^{-1}$ (SPE0, teal pentagons), $c_{LiTFSI} = 0.2\,mol\,kg^{-1}$ (SPE2, blue diamonds) and $c_{LiTFSI} = 0.5\,mol\,kg^{-1}$ (SPE5, green dots), respectively. For each sample, a temperature $T_{S,max}$ can be identified where $|S|$ reaches a maximum, indicating a balance between thermal activation and repulsive interaction of mobile ions for a given concentration, and decreases with increasing concentration c_{LiTFSI}. $T_{S,max}$ for the respective sample is indicated by arrows.

SPE5), lead to an even further increase of the Seebeck coefficient (S = (–1.93 ± 0.05) mV K^{-1}) at room temperature which is indicative for the situation of more mobile ions being available which, in turn, can build up a thermovoltage upon accumulation at the colder polymer-electrode interface. There are studies reporting larger Seebeck coefficients for ionic systems. However, these were mainly carried out on aqueous gels or ionic liquids, respectively. As such, Seebeck coefficients between 0.3 and 4.2 mV K^{-1} have been observed for aqueous PSS:Na gels, however, varying strongly with relative humidity.[23] Ionic Seebeck coefficients of –7.6 and 7 mV K^{-1} have been cited in refs. [24], [25], respectively. However, in these examples ionic liquids such as tetrabutylammonium nitrate in dodecanol were used, which are of minor, if at all, potential for practical TE applications. Furthermore, the maintenance of sufficiently large temperature gradients is expected to be difficult in these liquid materials due to convection effects. Besides its increase with LiTFSI salt concentration, the Seebeck coefficient of the three samples shows a different temperature behavior. In particular, there exists a distinct temperature $T_{S,max}$ at which the maximum absolute value $|S|_{max}$ is reached. Above $T_{S,max}$, the value of $|S|$ decreases again, presumably due to an thermally enhanced number of mobile ions, leading to stronger repulsive ion– ion interactions significantly affecting the ionic transport in the polymer electrolyte. An increase of the fraction of free ions has been reported for PEO/LiTFSI based on MD simulations.[26] In contrast to the absolute Seebeck coefficient, this crossover temperature decreases with increasing c_{LiTFSI}. For instance, $T_{S,max}$ is found to be around 320 K for sample SPE2 while it is reduced to $T_{S,max}$ = 290 K for SPE5. Concurringly, the higher number of TFSI$^-$ species upon increasing salt content renders more ions available for transport, thus, leading to an increase of $|S|$ already at lower temperatures, see for example, sample SPE5 versus SPE2. But counter-productive, the enhanced ion– ion interaction inherent to higher salt concentrations, will lead to a much steeper decline of $|S|$ toward higher temperatures.

2.2. Electrical Characterization

In a next step, to gain information on the contributing transport processes and their characteristic timescales, impedance measurements have been performed on the solid polymer electrolytes as function of LiTFSI concentration. For this purpose, two additional intermediate salt concentrations of c_{LiTFSI} = 0.1 mol kg^{-1} (SPE1) and c_{LiTFSI} = 0.17 mol kg^{-1} (SPE1.7) were analyzed. Representative data for sample SPE2 (c_{LiTFSI} = 0.2 mol kg^{-1}) measured at various temperatures (293, 303, 323, and 343 K) are displayed in **Figure 2**a. The corresponding Nyquist plots feature a semicircle for all temperatures as well as a straight, but inclined line toward lower frequencies. As the polymer electrolyte is sandwiched between two ion-blocking copper-electrodes, the impedance spectra for all samples were fitted using a Debye circuit with an additional series resistance R_S, schematically displayed in Figure 2b. All datasets can be well described by the properties of this electrical equivalent circuit (EEC) (black dashed lines in Figure 2a). Small derivations from the semi-circular behavior can be ascribed to our measurement setup where the current flow at the electrode edges is no longer normal to the surface and, accordingly, the homogeneity of current density is locally perturbed. This non-ideal capacitance geometry, in general, can be modeled by a constant phase element but was neglected to reduce the number of free fit parameters. Furthermore, this contribution is negligible for deducing the bulk conductivities which are derived under consideration of the cell geometry by the bulk resistance R_i. The ionic conductivity at room temperature for sample SPE2 (c_{LiTFSI} = 0.2 mol kg^{-1}) amounts to σ = (4.03 ± 0.12) × 10^{-4} S m^{-1}, which is in good agreement to literature values reported for thin membranes of this polymer electrolyte.[18] Ion conductivity is closely associated with the movement of the monomer sub-units of the polymer backbones as the charged species experience their local environment as more liquid-like, whereas on macroscopic length scales, the polymer electrolyte behaves like a solid.[16,27,28] In

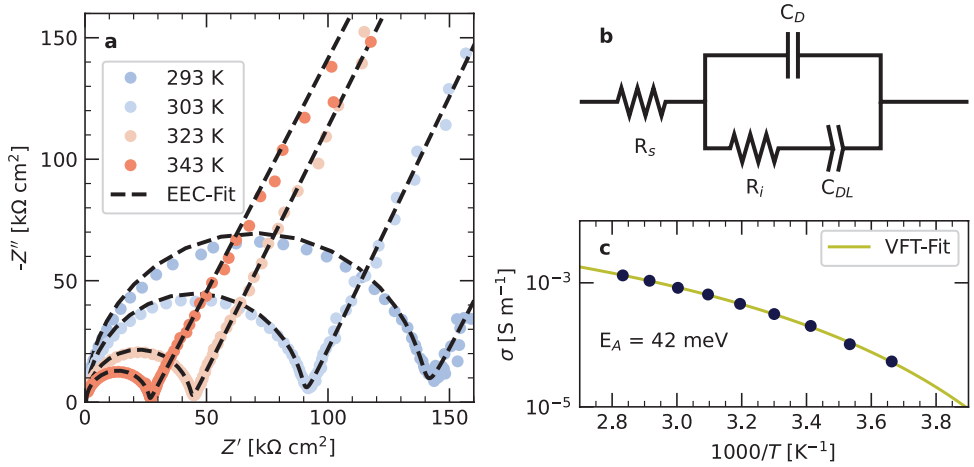

Figure 2. a) Temperature dependent Nyquist plots of a symmetrical Cu/solid polymer electrolyte/Cu cell. Measurements performed on a sample with c_{LiTFSI} = 0.1 mol kg^{-1}. Black dashed lines display the respective fits according to the electrical equivalent circuit shown in (b). Here, the sample is described by the dielectric capacitance C_D and a double layer capacitance C_{DL} connected in series with the bulk resistance R_i, which is related to the ionic conductivity σ for the given cell geometry. A resistance R_S was added in order to account for possible series resistances. c) Ionic conductivities in the polymer matrix derived from impedance spectra (blue dots). The thermal activation behavior can be described by a Vogel– Fulcher– Tammann (VFT) ansatz (green solid line) which yields an activation energy of E_A = (42 ± 5) meV and a Vogel temperature of T_V = (196 ± 7) K.

the PEGMA-based SPE under study, ionic conductivity is supported by ethoxy chains freely dangling within the matrix[29] and, hence, constituting the preferred segmental motion of the polymer. The temperature dependence of the ion conductivity in the disordered polymer matrix can therefore be expressed by the Vogel-Fulcher-Tammann (VFT)[30] formalism

$$\sigma = \sigma_0 \exp\left(-\frac{E_A}{k_b (T - T_v)}\right) \quad (1)$$

where T_v is the characteristic "Vogel temperature", interpreted as temperature where the segmental ion conductivity drops to zero,[16] and E_A is the effective activation energy of ionic movement, respectively. Figure 2c shows the temperature dependent ionic conductivity of sample SPE1 (c_{LiTFSI} = 0.1 mol kg^{-1}) with the complementary fit according to Equation (1). The activation energy for transport within the polymer electrolyte can be determined as E_A = (42 ± 5) meV with T_V = (196 ± 7) K. The $\sigma(T)$ curves for all samples under investigation are displayed together with their respective fits in Figure S2, Supporting Information; the corresponding effective activation energies E_A and Vogel temperatures T_V are summarized in Table S1, Supporting Information. The transport across the polymer matrix without LiTFSI additive (SPE0) can be expressed by a Vogel temperature of T_V = (226 ± 17) K and an activation energy of E_A = (21 ± 8) meV. By adding lithium salt to the polymer matrix and gradually increasing the concentration c_{LiTFSI}, more charge carriers are available that can contribute to charge transport and, thus, increase in conductivity. This contrasts with the rise in activation energy, E_A, caused by the increased ion– ion interaction. At the highest concentration (SPE5, c_{LiTFSI} = 0.5 mol kg^{-1}), the activation energy has risen to E_A = (87 ± 41) meV, whereas the Vogel temperature has declined to T_V = (149 ± 43) K (see also Figure S3, Supporting Information). The addition of salt, in general, leads to a stiffening of polymers as Li^+ supports crosslinking between the polymer chains. In our case, however, we expect the rather big anion as well as the ionic complexes to interfere with the crosslinking of the matrix, thus, leading to a "softening" of the polymers as indicated by the lower Vogel temperatures with increasing salt concentration. Similar observations of a decrease in the glass transition temperature T_g related to Vogel temperature T_V, upon addition of salt have been reported for poly(vinyl alcohol),[31] poly (vinylene carbonate),[32] and 1,3-diacetyl-4-imidazolin-2-one based electrolytes.[33]

According to both, molecular dynamic simulations as well as experimentally studies on polyether-based electrolytes, one lithium cation is coordinated with 4–6 oxygen atoms.[26,34,35] The ether group provides the coordinating sites to the cation for migration. By addition of salt the C—O—C stretching mode gets slightly shifted (shown for PEO-PAN/$LiPF_6$ by Arya et al. using Fourier transform infrared spectroscopy[36]) toward lower wavenumbers (i.e., lower energies) due to complexation of Li^+ with the ether group of the host polymer. A ratio of R = O/Li^+ for given concentrations was estimated (only the oxygen atoms in the repeating monomer units were considered). For the smallest concentration of c_{LiTFSI} = 0.1 mol kg^{-1} this ratio was estimated to R = 174 and for the highest concentration of c_{LiTFSI} = 0.5 mol kg^{-1} it was estimated to R = 35. Considering these ratios, especially in case of polymeric networks rather than spatially aligned linear polymer chains with multiple coordination sites of smaller distances, a reduction in R presumably leads to an increase in E_A. Furthermore, Arya et al., reported the previously mentioned red shift and a decrease in peak area corresponding to the C–O–C stretching mode. The decrease of peak area was ascribed to an increasing amorphous fraction in the host matrix.[36] Based on this observation, we assume that an initially higher amorphous fraction caused by sterically hindered crosslinking of the polymer chains will lead to lower Vogel temperatures and glass transition temperatures, respectively, as less energy is needed for polymer chains to reorganize on microscopic length scale.

2.3. Tuning Electrical Properties by Additon of Carbon Nanotubes

In a subsequent step, with the aim to combine the high Seebeck voltages and ionic conductivities, inherent to the investigated SPEs, with a high electronic contribution to the conductivity, we added multi-walled carbon nanotubes (MWCNTs) at defined ratio to the polymer electrolyte. Two samples were prepared with the same amount of 0.4 wt% MWCNTs in respect to the polymer, but with different salt concentrations of c_{LiTFSI} = 0.0 mol kg^{-1} and c_{LiTFSI} = 0.2 mol kg^{-1}. According to the previous notations, these samples will be denoted in the following as SPE0CNT and SPE2CNT, respectively. Although higher salt concentrations for example, c_{LiTFSI} = 0.5 mol kg^{-1} exhibit even larger Seebeck coefficients, salt solubility in the polymer matrix and resulting homogenous processability remain a challenge why a lower concentration (c_{LiTFSI} = 0.2 mol kg^{-1}) has been chosen for the investigations. Similar challenges regarding solubility occur for carbon nanotube additives, too, as their dispersion is limited to only small concentrations by the dramatic build up in viscosity. The aforementioned ratio of MWCNTs was chosen as a good compromise between increase in conductivity and viscosity. **Figure 3**a shows representative impedance spectra measured on sample SPE0CNT at temperatures of 273, 293, 323, and 353 K, respectively. The spectra clearly deviate from those presented above and can no longer be described by a Debye circuit with an additional series resistance. Despite resembling a semi-circle followed by a broad arc at low frequencies, the evident increase in conductivity by more than two orders of magnitude clearly distinguishes this sample from the polymer electrolyte of same LiTFSI salt concentration but without MWCNT additives (namely sample SPE0, see Figure S5, Supporting Information). Establishing a suited model to simulate the experimental data proves to be extremely difficult. Not only that each carbon nanotube within the matrix features an intrinsic resistance, the electrical transport between neighboring nanotubes has to be described by a contact resistance as well as a capacitance. Various other contributions to conductance or resistance, respectively, might play a role when considering a network of carbon nanotubes within a polymer matrix such as different dipolar and dielectric environments or carrier scattering at (charged) defects.[37] Hence, considering a disordered polymer matrix containing a large number of randomly oriented carbon nanotubes, the frequency dependent

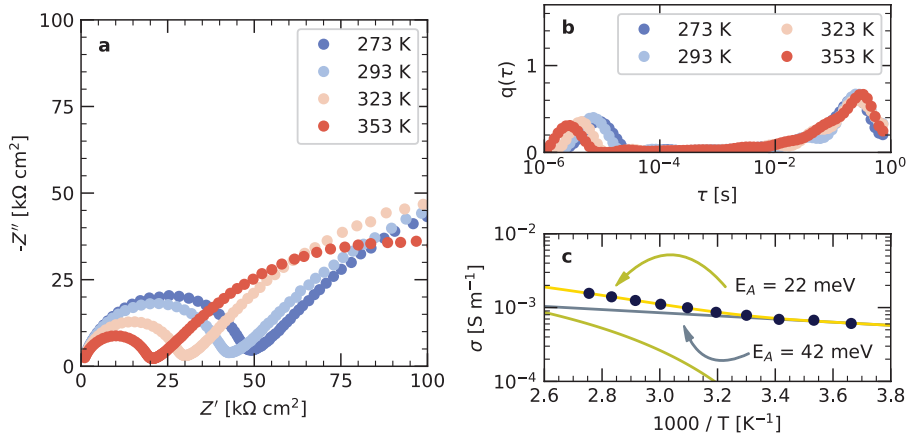

Figure 3. a) Nyquist plots of impedance data measured at 273, 293, 323, and 353 K for sample SPE0CNT (c_{LiTFSI} = 0.0 mol kg^{-1} and 0.4 *wt*% carbon nanotubes). The spectra clearly deviate from those before as the semi-circle and broad arc feature at low frequencies are characterized by an increase in conductivity by more than two orders of magnitude. b) Applying Tikhonov regularization, the DRT shows two clearly distinguishable agglomeration points. The first one, between $\tau = 10^{-6}$ to 10^{-5} s, shows a distinct temperature dependence. The second, smeared-out group at around $\tau = 10^{-1}$ s refers to a diffusive charge transport behavior. c) Conductivities derived from the first semi-circle of the impedance data (see also Figure S5, Supporting Information) plotted as a function of inverse temperature. The temperature dependent total conductivity σ (blue bullet points) can be modeled by overlapping Vogel– Fulcher– Tammann (green line) and Arrhenius type (gray line) transport models ($\sigma = \sigma_{VFT} + \sigma_{Arr.}$, yellow line), with VFT becoming dominant for higher temperatures. Fit results for the VFT contribution (E_a = (22 ± 14) meV, T_v = (249 ± 40) K) are in good agreement to the polymer-only sample (SPE0) without carbon nanotubes added. Obviously, a change in the dominant transport mechanism is evident at around T_c = 300 K. The Arrhenius type transport can be described by an activation energy of E_a = (42 ± 28) meV.

electrical response has to be modeled by a set of parallel RC-circuits connected in series, each of which can be characterized by a characteristic relaxation time $\tau = R \times C$. The overall impedance can then be described by a distribution of relaxation times τ (DRT) according to Equation (3) in Section 4. Further on, Tikhonov regularization was used as it allows impedance analysis without the need of specific information about the system under investigation and has widely succeeded in describing this class of problems.[38,39] The method was verified for impedance data gathered on samples SPE0 through SPE5 analyzed by EEC fitting (compare Figure S10, Supporting Information). The distribution of relaxation times composing the impedance spectra measured on sample SPE0CNT (shown in Figure 3a) are depicted in Figure 3b. Clearly, two relaxation time clusters can be identified in this distribution, one between $\tau = 10^{-6}$ to 10^{-5} s, which shows a pronounced temperature dependence that is not observable for the second, smeared out group of relaxation times at around $\tau = 10^{-1}$ s. The origin of the second feature is not fully understood yet, however it appears to be connected to processes with high activation energies related to the added carbon nanotubes. A Gaussian fitted to the first relaxation time cluster (which represents the largest contribution to the conductivity of the examined sample) yields a conductivity on the order of $\sigma = 10^{-3}$ S m^{-1}, which represents an increase by more than two orders of magnitude compared to the polymer only sample (SPE0). A representative fit based on the performed Tikhonov regularization is shown in Figure S5, Supporting Information. The conductivity is plotted in Figure 3c versus the inverse temperature. Two different transport regimes can be distinguished by the kink occurring at around 300 K. Assuming that both contributions, transport within the polymer and transport through the carbon nanotubes, respectively, play a role in the overall conductivity, a superimposed conductivity model comprising VFT as well as Arrhenius transport ($\sigma = \sigma_{VFT} + \sigma_{Arrhenius}$) has been used. Applying this model to the conductivity data of sample SPE0CNT (c_{LiTFSI} = 0.0 mol kg^{-1}, 0.4 *wt*% CNT) yields E_A = (22 ± 14) meV and T_V = (249 ± 40) K for the VFT contribution, which, regarding the fit errors, is in good agreement with the values obtained for sample SPE0. The Arrhenius type contribution yields an activation energy of E_A = (42 ± 28) K. A similar transition can be observed in the temperature dependent Seebeck coefficient S (compare Figure S7, Supporting Information). The positive Seebeck coefficient below T_c hints at holes to be the major charge carriers responsible for the electronic part of thermovoltage built-up. This might be due to intrinsic doping of the nanotubes and/or to doping by the dipolar environment, that is, by the oxygen atoms of the $TFSI^-$ anion or the polymer matrix. Above T_c, ionic contributions to the thermovoltage generated by the Soret effect gain dominance. This trend is additionally supported by the fact that the nanotubes exceeding the charge carrier mean free path in length are expected to limit the electronic transport by phonon scattering and structural defects,[37] thus leading to an overall decrease of charge carrier mobility with increasing temperature.[40] Two different contributions to the transport become also evident in sample SPE2CNT (c_{LiTFSI} = 0.2 mol kg^{-1}, 0.4 *wt*% CNT) (see Figure S6, Supporting Information). However, the transition temperature is decreased to around 280 K. As can be concluded, ionic transport dominates the overall conductivity above T_c whilst for temperatures below, the Arrhenius-like thermally activated transport along the carbon nanotubes plays the major role. Conductivity is increased by one order of magnitude compared to the SPE0CNT sample, yielding $\sigma = (8.4 \pm 1.0) \times 10^{-3}$ S m^{-1} at room temperature. The corresponding activation energy of the conductivity in the low temperature, that is, Arrhenius-like region amounts to E_A = (36 ± 212) meV. This value is in good

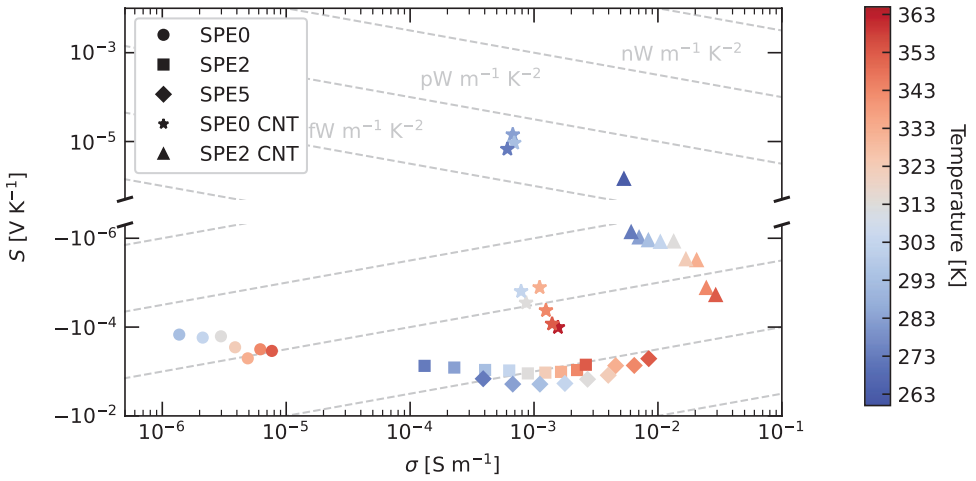

Figure 4. Seebeck coefficient S versus the bulk conductivity displayed in a symlog-log-plot. The y-axis is a symmetrical logarithmic axis with an axis break around zero thus allowing to display positive and negative values on a logarithmic scale. Gray dashed lines indicate iso-powerfactors as key parameter for TE application. Different samples are indicated by the respective shape of the data points; the temperature range for measurements (263–363 K) is color coded. Samples SPE0CNT and SPE2CNT, both containing carbon nanotubes, show a change in sign.

agreement with the activation energy for SPE0CNT at low temperatures, thus corroborating that transport in this regime is mainly governed by electronic charge movement along the carbon nanotubes. The pronounced error to the fit can be attributed to a very small number of points being close to the Arrhenius dominated transport regime. The high temperature regime, in contrast, is best described by the VFT ansatz with $T_V = (52 \pm 63)$ K and $E_A = (186 \pm 136)$ meV. Again, the characteristic parameters of transport, namely T_V and E_A, agree well with those of the corresponding sample without nanotubes, that is, SPE2, taking into account the respective error margins. Just like in the polymer electrolyte-only case, the Vogel temperature decreased upon the addition of salt. Still, it appears to be higher than in SPE2, which might be attributed to the MWCNT additive, the latter reducing the available free volume and, hence, increasing the glass transition temperature T_g. To demonstrate the broad parameter space in which the ionic and electronic transport parameters can be tuned by additives and temperature already in this work, the Seebeck coefficient S is plotted versus the conductivity σ in a symlog– log plot (see **Figure 4**). In this type of visualization, the y-axis is a symmetrical logarithmic axis with an axis break around zero thus allowing to display positive and negative values on the same logarithmic scale. Gray dashed lines indicate iso-power factors as the power factor (PF) is a key parameter for thermoelectric applications. Data gathered on five samples of different salt contents and different carbon nanotubes (SPE0, SPE2, SPE5 as well as SPE0CNT and SPE2CNT, respectively) in this work are plotted. Different measurement temperatures are color coded. By adding 0.2 mol kg^{-1} LiTFSI and 0.4 *wt*% MWCNTs the conductivity can be increased by four orders of magnitude. It has to be noted that the highest power factor in this work is achieved for polymer electrolytes without carbon nanotube additives, especially SPE5. However, the temperature dependent change in sign of the Seebeck coefficient in samples incorporating MWCNTs allows for possible new fields of application. Change of polarity in Seebeck coefficient has been reported,[41] however, with the necessity of adjustments in gel composition. In contrast, our approach allows a thermoelectric junction that can be switched on and off at a distinct temperature. To demonstrate this experimentally, we built a proof-of-concept single-junction thermoelectric generator based on 3:7 w/w PEGMA/BEMA with 0.2 mol kg^{-1} LiTFSI and 0.4 *wt*% MWCNTs, respectively. The device scheme is illustrated in **Figure 5**a. Well-known PEDOT:PSS was chosen as p-type conductor with a typically Seebeck coefficient in the range of $S \approx 10\,\mu V\,K^{-1}$. For temperatures above T_c the SPE behaves like an n-type conductor in terms of Seebeck coefficient S whereas below T_c it represents a p-type conductor, respectively, with a Seebeck coefficient in the range of $S \approx 1\,\mu V\,K^{-1}$. Thus, as both materials are connected thermally in parallel, it is possible to drastically reduce thermopower generated below T_c, since, due to the electrical series connection, the thermovoltages will nearly cancel each other. However, due to the fundamentally different nature of the generated voltages a TEG based on ionic systems operates slightly different than a purely electronic one.[23] Two concepts of operation are reported in literature for ionic based devices to generate current from an applied temperature gradient.[19] The presented device constitutes an example for using non-redox-reactive ions which accumulate at the colder electrolyte-electrode interface leading to an ionic thermoelectric supercapacitor. For demonstrating the general TEG-functionality different load resistances R_L have been connected in series and the occurring current was measured for 60 s. Typical discharge curves could be observed (compare Figure S8, Supporting Information). An effective output power was derived by integrating the currents at different temperatures T_{med} = 283, 313, and 343 K, respectively, and is shown in Figure 5b. A log– log-plot was chosen to clarify the effects related to the material properties described above. Employing only a single junction we reached a maximum power output of P_{out} = 13.63 nW at T = 343 K, which is more than three orders of magnitude higher than at T_{med} = 283 K. This cannot solely be explained by an increase in conductivity. For the SPE mixtures used in the TEG this should just give a factor of

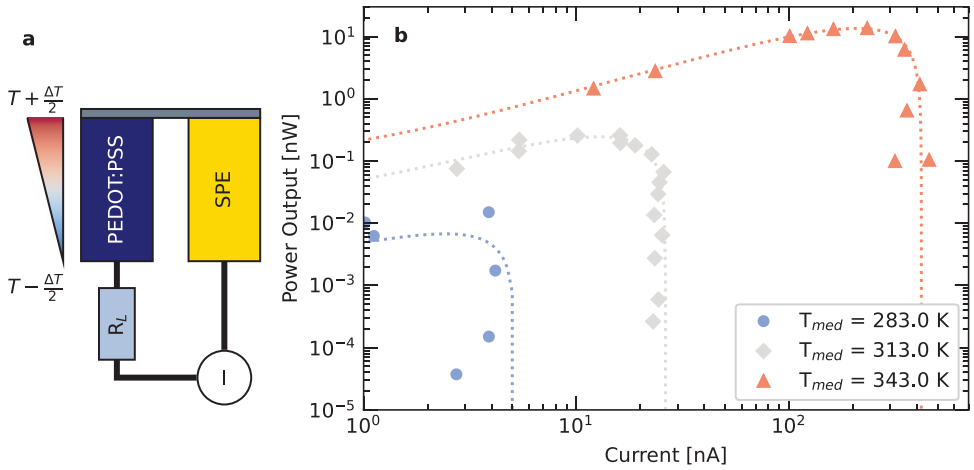

Figure 5. a) Scheme of the mixed electronic and ionic thermoelectric generator built as proof-of-concept device. A temperature difference of ΔT is applied across the two legs. The SPE leg contains a polymer blend with a concentration of $c_{LiTFSI} = 0.2\,mol\,kg^{-1}$ and 0.4 *wt*% of carbon nanotubes exhibiting a negative thermovoltage above $T_c = 303$ K, and a positive one below. The second PEDOT:PSS polymer leg shows a positive Seebeck coefficient. b) The power output characteristics for a temperature gradient of $\Delta T = 10$ K at different temperatures $T_{med} = 283$, 313, and 343 K is shown. To estimate the power output of the TEG various load resistances R_L have been connected in series and the occurring current flow has been measured and integrated for a duration of 60 s. The dashed lines are guide-to-the-eyes and indicate the trend in the data around T_{med}. The observed behavior corroborates an operational mode where the TEG can be switched on/off at T_{med}.

3.3 (compare Figure S6, Supporting Information). Even considering $P = I^2 \times R$ this appears to be an insufficient explanation. Instead, the observed behavior proves the possibility to switch the TEG on and off at a certain device temperature due to the change in sign of the Seebeck coefficient, hence, almost compensating the thermovoltage generated by PEDOT:PSS. This is supported by measurements at $T_{med} = 343$ K for various applied temperature gradients of $\Delta T = 10$, 20, and 30 K (compare Figure S9, Supporting Information). With increasing temperature difference, the effective output power decreases as the SPE is partially below the transition temperature of 330 K at which the sign of the Seebeck coefficient changes and hence reduces the effective thermovoltage. As the ionic contribution to thermovoltage mediated by the polymer is almost "frozen" out below the critical temperature T_c, the electronic contribution by the multi-walled carbon nanotubes becomes dominant in this temperature regime. Above T_c, ionic contributions to the thermovoltage generated by the Soret effect gain dominance. Hence, the new thermoelectric operation mode presented in our study would allow for temperature-activated control of different contributions to conductivity and, thus, thermoelectric transport. As a result, this would minimize or even avoid the need for microcontrollers or complex circuitry to control the various contributions extrinsically, and, thus, would facilitate the device architecture. Of course, the influence of ambient conditions (i.e., humidity or pressure) or chemical effects like solvent induced swelling of the polymer in case of gel-like electrolytes, needs to be investigated in more detail in future studies.

3. Conclusion

Thermovoltages were measured as a function of LiTFSI salt concentration indicating a sweet spot for a concentration of $c_{LiTFSI} = 0.2\,mol\,kg^{-1}$. The mechanism of ionic migration was investigated using temperature dependent impedance spectroscopy techniques. A VFT mechanism could be verified for all samples under investigation. Upon the addition of multi-walled carbon nanotubes, two different transport mechanisms were observed. The first, above a critical temperature T_c, was described by VFT formalism and mainly attributed to ionic and polymeric segmental mobility. The second, below the critical temperature, showed Arrhenius-like temperature activated hopping transport and is directly related to the added carbon nanotubes. The transition between the two distinct transport regimes could be correlated to a change in sign of the Seebeck coefficient. The two distinct operation modes promise TE devices that can be switched by ambient temperature. By optimized materials and composites in the future, the effect is expected to become more pronounced. However, more research has to be done on how to boost power factors by a couple of orders of magnitude. The presented work lays fundamental ground work for this research and results obtained substantiate the potential of mixed ionic and electronic materials for future low- and mid-temperature TE applications.

4. Experimental Section

Materials and Sample Preparation: PEGMA (M_n = 500) and BEMA (M_n = 1700) were obtained from Sigma Aldrich. Before their use, they were kept in the inert atmosphere of an Ar-filled dry glove box for a couple of days. PEGMA and BEMA were mixed in a 3:7 weight ratio. Different contents of LiTFSI (Sigma Aldrich) and MWCNT (Sigma Aldrich), respectively, were stirred into the polymer blend. 2–4 wt% of 2-hydroxy-2-methylpropiophenone was added as photo initiator. The polymer was filled in a test cell and solidified by UV curing (λ=400 nm) under inert gas atmosphere.

Determination of Transport Properties: Vertical cells of copper || SPE || copper were used for the measurement of (ionic) conductivities by means of impedance spectroscopy experiments in a temperature range

between 263 and 363 K. Experimental data were obtained using the Zurich Instruments MFIA impedance analyzer in a frequency range from 100 mHz to 510 kHz. Conductivities were calculated using Equation (2)

$$\sigma = L/(A \times R) \tag{2}$$

with L and A being thickness and area of the samples, respectively. R denotes the respective resistance, which was obtained from the impedance spectra. Thermoelectric measurements were performed in vertical cells of copper || SPE || copper of which the two sides could be heated/cooled independently using Peltier devices (Telemeter Electronics). By varying the temperature around a constant mean temperature, a temperature difference will give rise to the thermovoltage, which was recorded with a Keithley KE2182 A Nanovoltmeter. The Seebeck coefficient S can be determined from the slope of the measured voltage (U_{th}) versus the applied temperature difference (ΔT) curve.[42] Measurements are conducted continuously in quasi-steady state. Heating rates of 1 K min^{-1} and holding times of 30 s at a given temperature difference assure sufficient time to give rise to the steady-state thermovoltage.[43] The employed temperature difference was limited to ΔT_{max} = 10 K. The data obtained were corrected for the Seebeck coefficient of the contacting wire (Cu) which is well documented in literature[44] (S_{Cu} = 1.5 µV K^{-1} at room temperature). All above mentioned measurements were carried out under vacuum conditions ($p \approx$ 1–10 mbar).

Tikhonov Regularization: The complex impedance spectrum $Z(\omega)^* = Z(\omega)' + j \cdot Z(\omega)''$ described by real and imaginary parts $Z(\omega)'$ and $Z(\omega)''$, can also be represented by its frequency distribution, according to

$$Z(\omega)^* = R_S + R_P \int_{-\infty}^{+\infty} \frac{G(\log \tau)}{1 + j\omega\tau} d(\log \tau) \tag{3}$$

with the series resistance R_S, the total polarization resistance R_P, G the distribution of relaxations times (DRT), and $\tau = RC$ as the relaxation time. R and C are the effective resistance and capacitance, respectively and ω constitutes the angular frequency. Solving for the DRT is known as ill-posed inverse problem, for which the Tikhonov regularization is a versatile tool. Therefore, Tikhonov regularization was used as an alternative approach to interpret impedance spectroscopy data and to verify the chosen EEC, respectively. Data evaluation was performed using an *L*-curve approach coupled with the Tikhonov regularization as proposed in ref. [38] with a self-written Python code based on MATLAB regularization tools.[45] Method verification was performed on impedance data from samples SPE0– SPE5 (see Figure S10, Supporting Information).

Thermoelectric Generator: A prototype of a solid polymer electrolyte thermoelectric generator was built as depicted in Figure 5a consisting of one junction. The n-type leg was made of a UV-cured PEGMA/BEMA LiTFSI MWCNT blend of length L = 4 mm and cross section A = 0.75 cm^2. Poly(3,4-ethylenedioxythiophene) polystyrene sulfonate (PEDOT:PSS) dry-pellets (Sigma Aldrich) were re-dispersed and after evaporation of the solvent used for the p-leg (length L = 2 mm and cross-section A = 1 cm^2) as its (thermo)electric properties are well known. The two legs were connected by a copper block. Different temperature gradients had been applied to the TEG and the corresponding open-circuit voltages were measured. Afterwards a fixed ΔT was applied and different load resistances were used and the current passing through the respective load was measured by a Keithley KE6517A electrometer.

Supporting Information

Supporting Information is available from the Wiley Online Library or from the author.

Acknowledgements

The authors thank the Bavarian Ministry of Science and the Arts for the generous support by the research program *Solar Technologies Go Hybrid*.

Open access funding enabled and organized by Projekt DEAL.

Conflict of Interest

The authors declare no conflict of interest.

Data Availability Statement

The data that support the findings of this study are available from the corresponding author upon reasonable request.

Keywords

carbon nanotubes, electrochemistry, impedance spectroscopy, polymer electrolytes, thermoelectric characterization, thermoelectric generators

Received: March 22, 2022
Revised: May 6, 2022
Published online: May 31, 2022

[1] C. Forman, I. K. Muritala, R. Pardemann, B. Meyer, *Renewable Sustainable Energy Rev.* **2016**, *57*, 1568.
[2] G. S. Snyder, E. S. Toberer, *Nat. Mater.* **2008**, *7*, 105.
[3] M. Goel, M. Siegert, G. Krauss, J. Mohanraj, A. Hochgesang, D. C. Heinrich, M. Fried, J. Pflaum, M. Thelakkat, *Adv. Mater.* **2020**, *32*, 2003596.
[4] T. Ma, W. Kent, B. X. Dong, G. L. Grocke, S. N. Patel, *Appl. Phys. Lett.* **2021**, *119*, 013902.
[5] F. Huewe, A. Steeger, K. Kostova, L. Burroughs, I. Bauer, P. Strohriegl, V. Dimitrov, J. Pflaum, *Adv. Mater.* **2017**, *29*, 1605682.
[6] J. Wüsten, K. Potje-Kamloth, *J. Phys. D: Appl. Phys.* **2008**, *41*, 135113.
[7] S. Liu, H. Li, C. He, *Carbon* **2019**, *149*, 25.
[8] I. Petsagkourakis, K. Tybrandt, X. Crispin, I. Ohkubo, N. Satoh, T. Mori, *Sci. Technol. Adv. Mater.* **2018**, *19*, 836.
[9] O. Bubnova, Z. U. Khan, H. Wang, S. Braun, D. R. Evans, M. Fabretto, P. Hojati-Talemi, D. Dagnelund, J.-B. Arlin, Y. H. Geerts, S. Desbief, D. W. Breiby, J. W. Andreasen, R. Lazzaroni, W. M. Chen, I. Zozoulenko, M. Fahlman, P. J. Murphy, M. Berggren, X. Crispin, *Nat. Mater.* **2013**, *13*, 190.
[10] B. T. McGrail, A. Sehirlioglu, E. Pentzer, *Angew. Chem., Int. Ed.* **2015**, *54*, 1710.
[11] O. Bubnova, M. Berggren, X. Crispin, *J. Am. Chem. Soc.* **2012**, *134*, 16456.
[12] Y. Sun, P. Sheng, C. Di, F. Jiao, W. Xu, D. Qiu, D. Zhu, *Adv. Mater.* **2012**, *24*, 932.
[13] H. Wang, U. Ail, R. Gabrielsson, M. Berggren, X. Crispin, *Adv. Energy Mater.* **2015**, *5*, 1500044.
[14] X. He, H. Cheng, S. Yue, J. Ouyang, *J. Mater. Chem. A* **2020**, *8*, 10813.
[15] M. Bharti, A. Singh, A. K. Debnath, A. K. Chauhan, K. P. Muthe, S. K. Gupta, K. Marumoto, T. Mori, D. K. Aswal, *Mater. Today Phys.* **2021**, *16*, 100307.
[16] J. Mindemark, M. J. Lacey, T. Bowden, D. Brandell, *Prog. Polym. Sci.* **2018**, *81*, 114.
[17] A. Arya, A. L. Sharma, *Ionics* **2017**, *23*, 497.
[18] J. R. Nair, C. Gerbaldi, M. Destro, R. Bongiovanni, N. Penazzi, *React. Funct. Polym.* **2011**, *71*, 409.
[19] D. Zhao, A. Würger, X. Crispin, *J. Energy Chem.* **2021**, *61*, 88.
[20] M. Kühne, F. Paolucci, J. Popovic, P. M. Ostrovsky, J. Maier, J. H. Smet, *Nat. Nanotechnol.* **2017**, *12*, 895.
[21] P. Kurzweil, O. K. Dietlmeier, *Elektrochemische Speicher*, Springer Vieweg, Wiesbaden **2018**.

[22] N. Dubey, M. Leclerc, *J. Polym. Sci., Part B: Polym. Phys.* **2011**, *49*, 467.
[23] H. Wang, D. Zhao, Z. U. Khan, S. Puzinas, M. P. Jonsson, M. Berggren, X. Crispin, *Adv. Electron. Mater.* **2017**, *3*, 1700013.
[24] E. Laux, S. Uhl, N.Gauthier, L. Jeandupeux, H. Keppner, P. P. Lopez, S. Pauline, E. Vanoli, R. Marti, *Mater. Today: Proc.* **2018**, *5*, 10195.
[25] M. Bonetti, S. Nakamae, M. Roger, P. Guenon, *J. Chem. Phys.* **2011**, *134*, 114513.
[26] O. Borodin, G. D. Smith, *Macromolecules* **2006**, *39*, 1620.
[27] H. Porthault, G. Piana, J. M. Duffault, S. Franger, *Electrochim. Acta* **2020**, *354*, 136632.
[28] K. I. S. Mongcopa, M. Tyagi, J. P. Mailoa, G. Samsonidze, B. Kozinsky, S. A. Mullin, D. A. Gribble, H. Watanabe, N. P. Balsara, *ACS Macro Lett.* **2018**, *7*, 504.
[29] J. R. Nair, C. Gerbaldi, G. Meligrana, R. Bongiovanni, S. Bodoardo, N. Penazzi, P. Reale, V. Gentilli, *J. Power Sources* **2008**, *178*, 751.
[30] M. Armand, *Adv. Mater.* **1990**, *2*, 278.
[31] X. Wei, D. F. Shriver, *Chem. Mater.* **1998**, *10*, 2307.
[32] J. Chai, Z. Liu, J. Ma, J. Wang, X. Liu, H. Liu, J. Zhang, G. Cui, L. Chen, *Adv. Sci.* **2017**, *4*, 1600377.
[33] H. Mitsuda, T. Uno, M. Kubo, T. Itoh, *Polym. Bull.* **2006**, *57*, 313.
[34] O. Borodin, G. D. Smith, O. Geiculescu, S. E. Creager, B. Hallac, D. DesMarteau, *J. Phys. Chem. B* **2006**, *110*, 24266.
[35] Y. Duan, J. W. Halley, L. Curtiss, P. Redfern, *J. Chem. Phys.* **2005**, *122*, 054702.
[36] A. Arya, A. L. Sharma, *J. Mater. Sci.: Mater. Electron.* **2018**, *29*, 17903.
[37] N. F. Zorn, J. Zaumseil, *Appl. Phys. Rev.* **2021**, *8*, 041318.
[38] T. Paul, P. W. Chi, P. M. Wu, M. K. Wu, *Sci. Rep.* **2021**, *11*, 12624.
[39] L. E. Helseth, *Mater. Res. Express* **2018**, *5*, 105002.
[40] V. Perebeinos, J. Tersoff, P. Avouris, *Phys. Rev. Lett.* **2005**, *94*, 086802.
[41] D. Zhao, A. Martinell, A. Willfahrt, T. Fischer, D. Bernin, Z. U. Khan, M. Shahi, J. Brill, M. P. Jonsson, S. Fabiano, X. Crispin, *Nat. Commun.* **2019**, *10*, 1093.
[42] J. de Boor, E. Müller, *Rev. Sci. Instrum.* **2013**, *84*, 065102.
[43] K. A. Borup, J. de Boor, H. Wang, F. Drymiotis, F. Gascoin, X. Shi, L. Chen, M. I. Fedorov, E. Müller, B. B. Iversen, G. J Snyder, *Energy Environ. Sci.* **2015**, *8*, 423.
[44] F. J. Blatt, R. H. Kropschot, *Phys. Rev.* **1960**, *118*, 480.
[45] P. C. Hansen, *Numer. Algorithms* **2007**, *46*, 189.